LAP-based tracking for focal adhesions

Lomanov, K., Martinez del Rincon, J., Miller, P., & Gribben, H. (2018). LAP-based tracking for focal adhesions. In *Irish Machine Vision and Image Processing Conference Proceedings 2018: Proceedings* (pp. 49-56) https://iprcs.scss.tcd.ie/pdf/IMVIP2018Book.pdf#page=59

Published in:
Irish Machine Vision and Image Processing Conference Proceedings 2018: Proceedings

Document Version:
Peer reviewed version

LAP-based tracking for focal adhesions

Anonymous Submission

Anonymous Affiliation

Abstract

We present a focal adhesion (FA) detector and tracker based on an IMM algorithm combined with the double use of the linear assignment problem (LAP) for data association. Performance has been evaluated using a real confocal microscopy image sequence of a migrating NHEK stained for FAs. The tracker has been compared against several state-of-the-art, commercially available tracking algorithms. With a MOTA of 31.6, it outperforms each of these other methods.

Keywords: Focal Adhesion Tracking, Multiple Object Tracking, Particle Tracking, IMM Algorithm

1 Introduction

Gaining a deeper understanding of the biological processes that govern living cells is crucial to ensure progress in medicine. Observing mechanisms at such small scale used to be nearly impossible, but advances in microscopy techniques such as PALM, STORM, or STED have made possible to circumvent the diffraction limit [Cox, 2015, Hu et al., 2015, Godin et al., 2014], enabling biologists to observe processes at the nanometre scale in real time. Despite the numerous advantages, new challenges have also emerged. Indeed, the tremendous amount of images has rendered manual processing highly ineffective and made indispensable to develop automated analysis of live cell images [Möhl et al., 2012, Peng, 2008, Meijering et al., 2006].

Cell adhesion and migration are among the vital processes that could benefit from automated extraction and analysis. Cell migration is a driving force behind many biological mechanisms, including immune responses and wound healing, and its improper functioning can trigger life threatening issues, such as tumors and autoimmune diseases [Etienne-Manneville, 2008, Gurtner et al., 2008]. The process of cell adhesion has an essential role in cell migration and heavily relies on subcellular protein structures called focal adhesions (FAs) [Strzyz, 2016], hence the importance of quantitatively analysing the latter. Nevertheless, FAs can display a multiplicity of complex behaviours, including changing shape, assembling, disassembling or sliding [Ballestrem et al., 2001], thus making their tracking a challenging task. This variety in behaviour and appearance as well as the difficulty to reliably segment them call for the use of one or several carefully chosen motion models to effectively extract their trajectory.

We propose in this paper the use of probabilistic tracking algorithms to accurately and robustly track focal adhesions moving inside a single NHEK migrating in a 2D environment. In particular, the use of the Interacting Multiple Model (IMM) algorithm [Blom and Bar-Shalom, 1988] is proposed given its ability to take into account several different motion models at every given time. We formulate the data association problem as two linear assignment ones.

The proposed algorithm is evaluated using a real confocal microscopy image sequence of focal adhesions, and compared to several state-of-the-art focal adhesion tracking algorithms.

2 Related Work

Focal adhesion (or other particle) tracking was, until recently, mostly done either manually [Owen et al., 2007, Webb et al., 2004] or using deterministic methods [Meijering et al., 2006, Berginski et al., 2011]. Manual approaches involve hand-picking a few significant particles and performing all the measurements only on them, while neglecting the bulk of the data. This can be extremely time-consuming even for such partial datasets and, most importantly, it does not use all the available information, which can lead to incomplete or wrong conclusions, as well as adding the subjectivity of human annotation.

As an alternative, automatic deterministic approaches have been proposed based on tracking by detection. Such approaches usually consist of two main steps: first particle detection is performed on each frame, and then data association temporally links particles over the frames to obtain complete tracks. These approaches therefore heavily rely on the quality of the detection step. Although a deterministic approach can yield decent results in applications with more easily distinguishable objects (such as animals or vehicles) and higher quality images, it is rarely suitable for biology applications due to their generally low signal to noise ratio and the identical appearance of the multiple particles to be tracked. These approaches are also impacted by the lack of specific and reliable FA detectors, therefore relying on general purpose segmentation such as simple thresholding, the watershed transform [Meijering et al., 2006] or wavelet transform [Genovesio et al., 2006].

Quite a few probabilistic tracking algorithms have been proposed for particle tracking [Jaqaman et al., 2008, Genovesio et al., 2006], using the likes of the KF [Kalman, 1960], IMM algorithm [Blom and Bar-Shalom, 1988], particle filter [Doucet and Johansen, 2011], or Multiple Hypothesis Tracking [Blackman, 2004]. Better results are achieved with such approaches, because they allow for an imperfect segmentation, which is often the case in biology images, and they allow us to introduce several motion models, used to solve uncertainty between identical particles.

Very few methods have been specifically developed for tracking focal adhesions. For instance, PAASTA [Broussard et al., 2015] performs tracking by linking detections using a simple nearest neighbour algorithm. Focal Adhesion Analysis Server (FAAS) [Berginski et al., 2011], and [Würflinger et al., 2011] link them by using an overlap criterion instead. However, none of them exploits the advantages of probabilistic tracking.

3 Methods

In this section we present our overall system for detecting and tracking FAs. A double step data association framework is used to orchestrate the tracking and combine multiple motion model predictions with the focal adhesion detections into the final estimated tracks. The architecture is depicted in Figure 1.

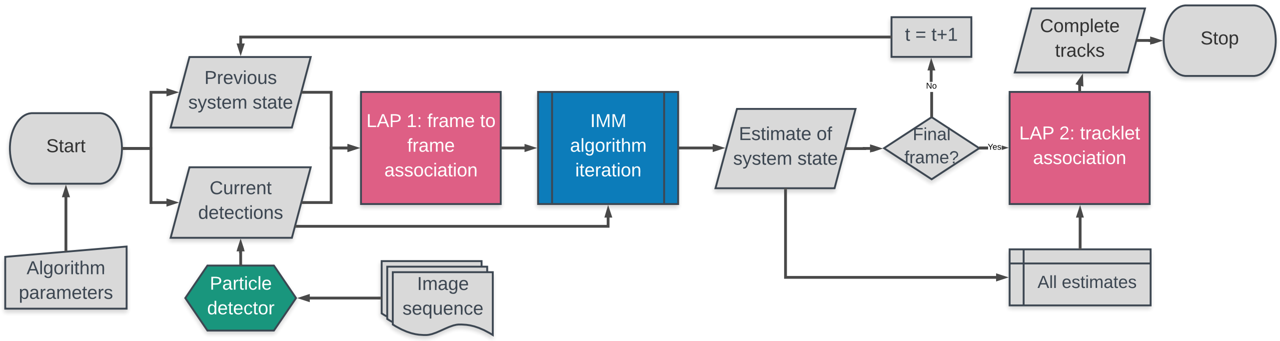

Figure 1: Flowchart of the proposed algorithm.

3.1 Detection

The shapes of focal adhesions vary with time and location, but can reasonably be approximated by ellipses of different excentricities [Hu et al., 2015]. To extract the location, size and orientation of the FAs, we use a strategy similar to [Würflinger et al., 2011]. Each image is processed using the steps described in Figure 2.

The image is first normalized, then smoothed using anisotropic diffusion. The background is removed using a morphological tophat transform with a size 12 disk as structuring element. This is followed by an Otsu binarization with 256 histogram bins. Finally, the individual ellipses are fitted to split the bigger FA clusters.

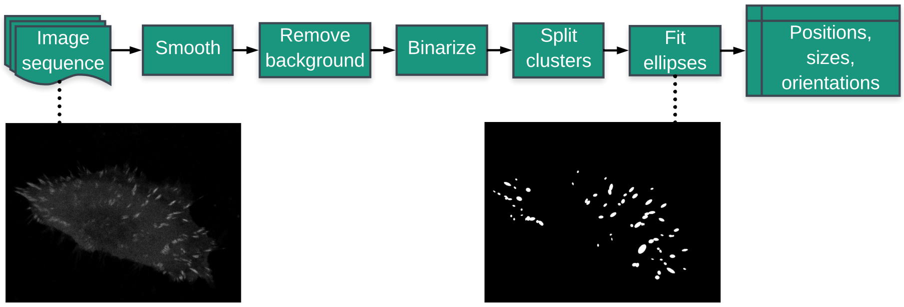

Figure 2: Flowchart of the FA detection.

3.2 Interacting Multiple Model algorithm

The state X_k of each FA at a given time step k is estimated using the IMM algorithm. The IMM combines state estimations from several dynamic models, corresponding to different Kalman filters. This allows for the consideration of each possible motion model for a tracked particle at each time step, and switching between them according to the current observations. Its flow diagram is shown in Figure 3.

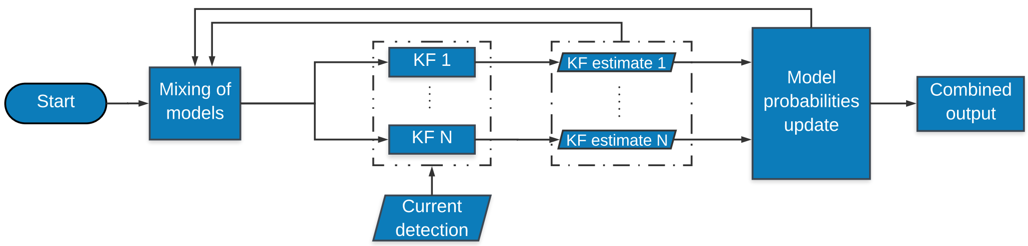

Figure 3: Flowchart of IMM algorithm.

Each considered dynamic model is represented by a transition matrix D^j for $j \in [\![1, N]\!]$, to model N possible behaviours for the particles. If a particle has an estimated state $\hat{X}_k$ and uncertainty $\hat{C}_k$ at the time step k, then the N predictions for the current time step $k+1$ are given by the equations 1:

$$X^j_{\text{pred},k+1} = D^j \tilde{X}^j_k \qquad\qquad C^j_{\text{pred},k+1} = D^j \tilde{C}^j_k {D^j}^T + Q_j \tag{1}$$

where Q_j is the process noise covariance for the model j, and the mixed state and covariance $\tilde{X}^j_k$ and $\tilde{C}^j_k$ are computed using the equations 2:

$$\tilde{X}^j_k = \sum_{i=1}^{N} u_k^{i|j} \hat{X}^i_k \qquad\qquad \tilde{C}^j_k = \sum_{i=1}^{N} u_k^{i|j} \left[\hat{C}^i_k + \left(\hat{X}^i_k - \tilde{X}^i_k\right)\left(\hat{X}^i_k - \tilde{X}^i_k\right)^T \right] \tag{2}$$

with $u_k^{i|j} = \frac{1}{u^j_{\text{pred},k+1}} p_{ij} u^i_k$ the conditional model probability, $u^j_{\text{pred},k+1} = \sum_{i=1}^{N} p_{ij} u^i_k$ the predicted model probability, and p_{ij} the probability to switch from the i^{th} to the j^{th} model from k to $k+1$.

Each prediction j is compared at current time $k+1$ against the observation Z_{k+1}, provided by the particle detection algorithm, to validate the relevance of the motion model j, using the Kalman equations 3.

$$\hat{X}^j_{k+1} = X^j_{\text{pred},k+1} + G^j_{k+1}\left(Z_{k+1} - H X^j_{\text{pred},k+1}\right) \qquad\qquad \hat{C}^j_{k+1} = C^j_{\text{pred},k+1}\left(I - G^j_{k+1} H\right) \tag{3}$$

The Kalman gain is defined by $G^j_{k+1} = C^j_{\text{pred},k+1} H^T \left(H C^j_{\text{pred},k+1} H^T + R\right)^{-1}$, where I is the identity matrix, H the observation matrix, and R the observation noise covariance.

The IMM then computes the estimated state and covariance of the particle as a weighted average of the individual estimates (equations 4).

$$\hat{X}_{k+1} = \sum_{j=1}^{N} u^j_{k+1} \hat{X}^j_{k+1} \qquad\qquad \hat{C}_{k+1} = \sum_{j=1}^{N} u^j_{k+1} \left[\hat{C}^j_{k+1} + \left(\hat{X}^j_{k+1} - \hat{X}_{k+1}\right)\left(\hat{X}^j_{k+1} - \hat{X}_{k+1}\right)^T \right] \tag{4}$$

The model probability u^j_{k+1} used in equations 4 is a normalised factor proportional to the likelihood for the model j:

$$u^j_{k+1} = \frac{1}{\sum\limits_{i=1}^{N} u^i_{\text{pred},k+1}\lambda^i_{k+1}} u^j_{\text{pred},k+1}\lambda^j_{k+1} \tag{5}$$

where the likelihood is given by $\lambda^j_{k+1} = \frac{1}{\sqrt{\det\left(2\pi S^j_{k+1}\right)}} \exp\left(-\frac{1}{2}\left(Z_{k+1} - HX^j_{\text{pred},k+1}\right)^T \left(S^j_{k+1}\right)^{-1} \left(Z_{k+1} - HX^j_{\text{pred},k+1}\right)\right)$, and S^j_{k+1} is defined as the covariance of the innovation of the j-th Kalman filter.

The update of these model probabilities at each time step allows the IMM to take into account the variations in the particle's behaviour over time and effectively track it.

3.3 Data association

3.3.1 Linear assignment problem

When dealing with multi-object tracking, it is essential to correctly assign observations to predictions and to minimise identity swapping. Following the successful strategy of [Jaqaman et al., 2008], this can be mathematically formulated as two linear sum assignment problems (LAP).

LAP is traditionally solved using the Hungarian method [Munkres, 1957], which is effective for applications involving only a few hundred particles per frame, as is the case in our FA application.

3.3.2 Frame-to-frame association (LAP1)

Let's consider the frame-to-frame linking step between frames k and $k+1$. The goal is to assign the N observations $\{Z_{k+1}\}_n$ for $n \in [\![1,N]\!]$ to the M trackers $\{\widehat{X}_{k+1}\}_m$ for $m \in [\![1,M]\!]$ so that the assignment ϕ is such that $\sum_{i=1}^{P} c_{i,\phi(i)}$ is minimal, with the $P \times P$ cost matrix $C = (c_{i,j})$ such as $c_{i,j}$ is the cost of associating the observation j to the tracker i, conventionally a square distance. If $N = M$, then $P = M = N$, otherwise $P = M + N$. All the links whose cost is above cut-off value CO_1 are excluded.

If no observation is assigned to a tracker for a certain number of consecutive frames MAMG, the tracklet is terminated. Non-assigned detections are used to initialize a new tracklet.

3.3.3 Tracklet association (LAP2)

The same method is applied for gap closing between tracklets, where the cost between tracklets is the square distance between the ending location of one and the starting location of the other. All the links above cut-off value CO_2 are excluded. When a tracklet is assigned to no other tracklet, it is considered a full track. This step is essential for recovering broken tracks and thus reducing the number of ID switches.

4 Experimental Results

4.1 Experimental setup

The state vector contains the current (x, y, z) positions of the ellipse centres at three consecutive frames, in order to have access to the velocity and acceleration of the FAs. This results in the following state vector:

$$X_k = (x_k, y_k, z_k, x_{k-1}, y_{k-1}, z_{k-1}, x_{k-2}, y_{k-2}, z_{k-2})^T$$

Our IMM implementation includes three motion models, all widely used for intracellular particle tracking [Genovesio et al., 2006]: Constant Velocity (CV), Constant Acceleration (CA), and Brownian Motion (BM). Process and measurement noise covariances Q_i and R are respectively set to the following values in all our experiments: $Q_{\text{CV}} = I_9$, $Q_{\text{CA}} = I_9$, $Q_{\text{BM}} = \text{diag}_9(1000)$, $R = \text{diag}_3(400)$. The default cut-off values for the first and second steps of the data association are respectively $CO_1 = 100$ and $CO_2 = 300$.

Multiple Object Tracking Accuracy (MOTA) is used for evaluation, developed specifically for multi-object tracking, and successfully used for several applications [Brendel et al., 2011, Benfold and Reid, 2011]. While their use in medical imaging is not very common, their advantage to measure all error types versus precision and recall are clear [Bernardin and Stiefelhagen, 2008].

MOTA aims to determine the tracker's ability to trace object trajectories, producing exactly one trajectory per object.

Thus, it is maximal when the sum of the false positives, misses, and mismatches IDS, divided by the total number of real objects GT is minimal. It is given by $\mathrm{MOTA} = 1 - \frac{\sum_t (\mathrm{FN}_t + \mathrm{FP}_t + \mathrm{IDS}_t)}{\sum_t \mathrm{GT}_t}$.

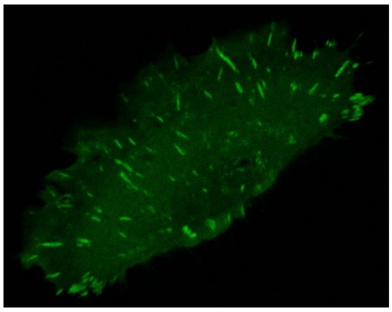

Figure 4: NHEK stained for FAs.

A dataset was recorded using confocal microscopy of a single cell, stained for vinculin to make FAs visible (see Figure 4). It consists of 48 frames, taken at 10 minute long intervals. FA centers were manually groundtruthed on each frame, resulting in 176 tracks.

4.2 Comparison with existing FA tracking frameworks

We compute the MOTA for several different FA tracking methods for comparison. In each case, their parameters were optimised to maximise the MOTA.

Ilastik [Sommer et al., 2011] is an open-source software for image analysis. We used its Automatic Tracking Workflow with our detections as input to compare the performances under equal detection conditions. FAAS is a web tool for both FA detection and tracking. A preprocessed sequence (smoothing and tophat transform) was used instead of the raw one for FAAS, since its segmentation was failing otherwise.

Table 1 shows the compared performances of all three systems, as well as the errors introduced by the detection algorithms alone. Resulting tracks are showed in Figure 5.

Tracker	Detection	FPs	FNs	ID sw	MOTA
Proposed	Proposed	1057	1918	**75**	**31.6**
Ilastik	Proposed	**794**	2533	196	21.0
Proposed	FAAS	2193	**1269**	117	19.7
FAAS	FAAS	2022	1427	303	15.8
-	Proposed	1014	2107	-	-
-	FAAS	1893	1679	-	-

Table 1: Comparison with other trackers.

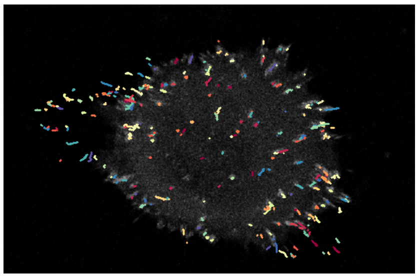

Figure 5: Obtained tracks.

Our combination of detection and tracking outperforms the two other ones by 50%, due in particular to a very low number of ID switches. Our tracker performs better than the other ones for a given detection method (be it our proposed detection or FAAS). Besides, our proposed detection also surpasses FAAS due to a lower sum of FNs and FPs.

4.3 Influence of the motion models used

In this experiment, different motion models and combinations are used in our framework to establish the most suited approach for tracking FAs. Given the little literature on automatic FA tracking and their complex behaviour, interesting conclusions could be obtained from this ablation experiment.

Results are shown in Table 2. The CV model performs best in terms of MOTA. The CA model seems to have little or detrimental effect. As for the BM model, it seems to reduce ID switches by allowing more random changes of direction, useful for unexpected cell behaviours, but it also increases the number of FNs and FPs due to less precise predictions. We have therefore chosen to only use the CV model for our final system.

CV	CA	BM	FPs	FNs	ID sw	MOTA
Yes	Yes	Yes	1075	1930	83	30.7
Yes	No	Yes	1076	1932	71	30.9
No	No	Yes	1074	1930	**66**	31.1
Yes	No	No	**1057**	**1918**	75	**31.6**
No	Yes	No	1078	1946	90	30.1

Table 2: Motion models ablation experiment.

4.4 Influence of the maximum accepted measurement gap

The MAMG is the maximum number of consecutive absent detections for a given track, above which the track is terminated. MOTA results for different gap values are shown in Figure 6 and Table 3.

MAMG	0	1	2	3	4	5	6	7	8
MOTA	30.8	**31.6**	30.3	30.6	29.7	28.5	27.3	26.4	24.4

Table 3: MOTA for different gaps.

When the MAMG increases, the number of ID switches decreases, because instead of starting a new tracklet, some new detections may be assigned to an existing one.

On the other hand, the FPs increase, while the FNs decrease. These are also expected consequences: while some of the tracklets correspond to proper misdetections and are corrected, other tracklets are instead artificially kept alive and do not correspond to any real FA.

As a consequence, the value of the maximum gap needs to be carefully chosen to maximise the MOTA, which is why we chose a gap of 1.

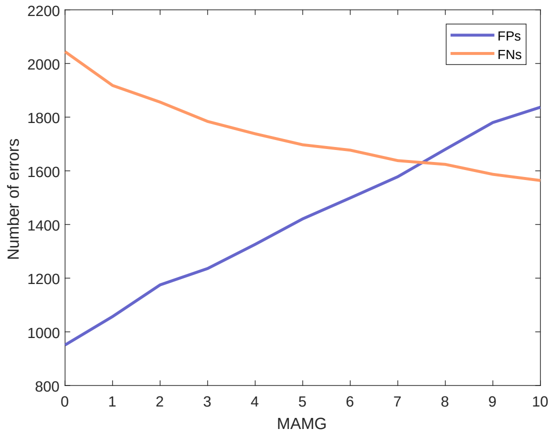

Figure 6: Errors for different MAMG values.

4.5 Influence of the percentage of misdetections

For this experiment, we simulated misdetections by using the ground truth as detections for tracker input, and randomly deleting different percentages of detections. This shows us the theoretical upper limit to the tracker's performance in isolation. Results are summarized in Figure 7.

The MOTA decreases following linear portions with the increase in misdetections. Overall it is quite robust to FNs, as long as the number of undetected particles remains reasonable. This highlight and its comparison against the real detectors underlines the importance of having a decent detector.

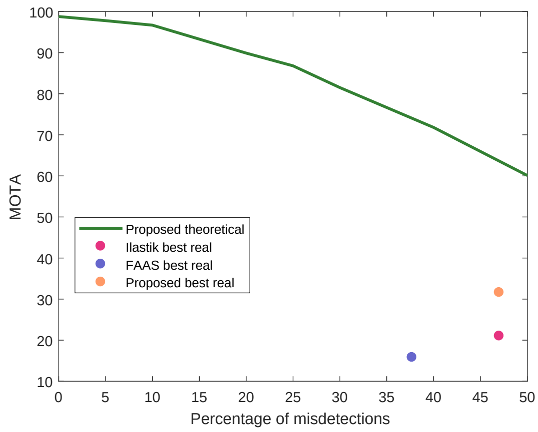

Figure 7: MOTA as a function of misdetections.

5 Conclusion

In this paper, we have described an algorithm for focal adhesion tracking, which uses an IMM method with a two-step LAP-based data association. The performance of the algorithm has been tested and compared to several state-of-the-art FA trackers, using real images. Our proposed system outperforms the other ones in terms of MOT CLEAR metrics.

For future work, we would like to investigate more FA segmentation methods to extract precise information and use it to improve data association costs.

Acknowledgments

This work has received funding from the European Union's Horizon 2020 research and innovation programme under the Marie Skłodowska-Curie grant agreement No 642866. We thank Galiya Sakaeva from FZJ for the data and Dmytro Kotsur from SCCH for the detection algorithm.

References

[Ballestrem et al., 2001] Ballestrem, C., Hinz, B., Imhof, B. A., and Wehrle-Haller, B. (2001). Marching at the front and dragging behind: differential $\alpha v\beta 3$-integrin turnover regulates focal adhesion behavior. *J Cell Biol*, 155(7):1319–1332.

[Benfold and Reid, 2011] Benfold, B. and Reid, I. (2011). Stable multi-target tracking in real-time surveillance video. In *Computer Vision and Pattern Recognition (CVPR), 2011 IEEE Conference on*, pages 3457–3464. IEEE.

[Berginski and Gomez, 2013] Berginski, M. E. and Gomez, S. M. (2013). The focal adhesion analysis server: a web tool for analyzing focal adhesion dynamics. *F1000Research*, 2.

[Berginski et al., 2011] Berginski, M. E., Vitriol, E. A., Hahn, K. M., and Gomez, S. M. (2011). High-resolution quantification of focal adhesion spatiotemporal dynamics in living cells. *PloS one*, 6(7):e22025.

[Bernardin and Stiefelhagen, 2008] Bernardin, K. and Stiefelhagen, R. (2008). Evaluating multiple object tracking performance: the clear mot metrics. *EURASIP Journal on Image and Video Processing*, 2008(1):1–10.

[Blackman, 2004] Blackman, S. S. (2004). Multiple hypothesis tracking for multiple target tracking. *IEEE Aerospace and Electronic Systems Magazine*, 19(1):5–18.

[Blom and Bar-Shalom, 1988] Blom, H. A. P. and Bar-Shalom, Y. (1988). The interacting multiple model algorithm for systems with markovian switching coefficients. *IEEE Transactions on Automatic Control*, 33(8):780–783.

[Brendel et al., 2011] Brendel, W., Amer, M., and Todorovic, S. (2011). Multiobject tracking as maximum weight independent set. In *Computer Vision and Pattern Recognition (CVPR), 2011 IEEE Conference on*, pages 1273–1280. IEEE.

[Broussard et al., 2015] Broussard, J. A., Diggins, N. L., Hummel, S., Georgescu, W., Quaranta, V., and Webb, D. J. (2015). Automated analysis of cell-matrix adhesions in 2d and 3d environments. *Scientific reports*, 5:8124.

[Cox, 2015] Cox, S. (2015). Super-resolution imaging in live cells. *Developmental biology*, 401(1):175–181.

[Doucet and Johansen, 2011] Doucet, A. and Johansen, A. M. (2011). *A tutorial on particle filtering and smoothing: fifteen years later*, chapter 24, pages 656–704. Oxford Handbook of Nonlinear Filtering. Oxford University Press.

[Etienne-Manneville, 2008] Etienne-Manneville, S. (2008). Polarity proteins in migration and invasion. *Oncogene*, 27(55):6970–6980.

[Everingham et al., 2010] Everingham, M., Van Gool, L., Williams, C. K., Winn, J., and Zisserman, A. (2010). The pascal visual object classes (voc) challenge. *International journal of computer vision*, 88(2):303–338.

[Genovesio et al., 2006] Genovesio, A., Liedl, T., Emiliani, V., Parak, W. J., Coppey-Moisan, M., and Olivo-Marin, J.-C. (2006). Multiple particle tracking in 3-d+t microscopy: Method and application to the tracking of endocytosed quantum dots. *IEEE Transactions on Image Processing*, 15(5):1062–1070.

[Godin et al., 2014] Godin, A. G., Lounis, B., and Cognet, L. (2014). Super-resolution microscopy approaches for live cell imaging. *Biophysical journal*, 107(8):1777–1784.

[Gurtner et al., 2008] Gurtner, G. C., Werner, S., Barrandon, Y., and Longaker, M. T. (2008). Wound repair and regeneration. *Nature*, 453(7193):314–321.

[Hu et al., 2015] Hu, S., Tee, Y.-H., Kabla, A., Zaidel-Bar, R., Bershadsky, A., and Hersen, P. (2015). Structured illumination microscopy reveals focal adhesions are composed of linear subunits. *Cytoskeleton*, 72(5):235–245.

[Jaqaman et al., 2008] Jaqaman, K., Loerke, D., Mettlen, M., Kuwata, H., Grinstein, S., Schmid, S. L., and Danuser, G. (2008). Robust single particle tracking in live cell time-lapse sequences. *Nature methods*, 5(8):695–702.

[Kalman, 1960] Kalman, R. E. (1960). A new approach to linear filtering and prediction problems. *Journal of Basic Engineering*, 82(1):35–45.

[Meijering et al., 2006] Meijering, E., Smal, I., and Danuser, G. (2006). Tracking in molecular bioimaging. *IEEE Signal Processing Magazine*, 23:46–53.

[Möhl et al., 2012] Möhl, C., Kirchgessner, N., Schäfer, C., Hoffmann, B., and Merkel, R. (2012). Quantitative mapping of averaged focal adhesion dynamics in migrating cells by shape normalization. *J Cell Sci*, 125(1):155–165.

[Munkres, 1957] Munkres, J. (1957). Algorithms for the assignment and transportation problems. *Journal of the society for industrial and applied mathematics*, 5(1):32–38.

[Owen et al., 2007] Owen, K. A., Pixley, F. J., Thomas, K. S., Vicente-Manzanares, M., Ray, B. J., Horwitz, A. F., Parsons, J. T., Beggs, H. E., Stanley, E. R., and Bouton, A. H. (2007). Regulation of lamellipodial persistence, adhesion turnover, and motility in macrophages by focal adhesion kinase. *The Journal of cell biology*, 179(6):1275–1287.

[Peng, 2008] Peng, H. (2008). Bioimage informatics: a new area of engineering biology. *Bioinformatics*, 24(17):1827–1836.

[Sommer et al., 2011] Sommer, C., Straehle, C., Koethe, U., and Hamprecht, F. A. (2011). Ilastik: Interactive learning and segmentation toolkit. In *Biomedical Imaging: From Nano to Macro, 2011 IEEE International Symposium on*, pages 230–233. IEEE.

[Strzyz, 2016] Strzyz, P. (2016). Cell migration: recycling active integrin for adhesion reassembly. *Nature Reviews Molecular Cell Biology*, 17(5):264.

[Webb et al., 2004] Webb, D. J., Donais, K., Whitmore, L. A., Thomas, S. M., Turner, C. E., Parsons, J. T., and Horwitz, A. F. (2004). Fak–src signalling through paxillin, erk and mlck regulates adhesion disassembly. *Nature cell biology*, 6(2):154.

[Würflinger et al., 2011] Würflinger, T., Gamper, I., Aach, T., and Sechi, A. (2011). Automated segmentation and tracking for large-scale analysis of focal adhesion dynamics. *Journal of microscopy*, 241(1):37–53.